Robust Kalman Filter for RTK Positioning under Signal-Degraded Scenarios

Haoqing Li¹, Daniel Medina², Jordi Vilà-Valls³, and Pau Closas¹

¹Dept. of Electrical & Computer Engineering, Northeastern University, Boston MA, USA
²Institute of Communications and Navigation, German Aerospace Center (DLR), Germany
³Institut Supérieur de l'Aéronautique et de l'Espace (ISAE-SUPAERO), University of Toulouse, France

INTRODUCTION

Location-based services, alongside with the modern applications on Intelligent Transportation Systems require reliable, continuous and precise navigation, positioning and timing information for their successful operation and implantation in the market. Global Navigation Satellite Systems (GNSS) constitute the backbone and main information supplier for Positioning, Navigation and Timing (PNT) data [1, 3, 4]. Despite offering a fairly good open sky positioning performance, standard differential code-based GNSS techniques can only achieve metre-level accuracy. Therefore, the accuracy potential for this approach is nearly exhausted and the transition techniques based on carrier phase observations is required in order to reach below decimetre-level positioning accuracies. Depending on the set of correction data, two kind of phase-based positioning techniques can be distinguished. First, Precise Point Positioning (PPP) reaches high accuracy by modelling GNSS system errors, such as ionospheric or tropospheric delays. PPP performance relies on GNSS satellite clock and orbit corrections, generated from a global network of stations. Although no nearby base station is required, which may be an advantage for some applications, the convergence time for the atmospheric corrections require from 5 to 20 minutes [10], excessive for safety-critical applications. Second, Real Time Kinematic (RTK) is a relative positioning procedure, where the position of a - potentially moving - receiver is determined with respect to a stationary base station of accurately known coordinates [5]. Thus, whenever the communication channel from the base station to the vehicle is sufficient, centimetre-level positioning accuracy can be reached almost immediately. Besides the interest of PPP techniques, this work focuses on RTK positioning and the challenges on urban navigation, where multipath effects can heavily deteriorate the navigation solution.

In RTK, the typical process to convert observables into position, velocity, and time (PVT) estimates involves some sort of state estimation problem. This is in general approach by solving a least-squares (LS) problem, or its recursive version resulting in the implementation of variants of the Kalman filter (KF). In such LS problem, both code and phase pseudoranges are exploited, then a vector of double-difference ambiguities must be estimated together with the targeted receiver position. Given the integer nature of such ambiguities, a possible solution is to use a three step approach. These are applied sequentially: i) float solution determination, ii) integer ambiguity fixing, and iii) state reconstruction. In the initial step, either a LS or KF-type method is considered, the ambiguities and other unknowns are estimated as real numbers (therefore, the results is often referred to as the *float solution*). Then, the estimated float ambiguities and the corresponding covariance matrix are used to obtain the integer ambiguities estimates. Finally, the computed integer ambiguities are used to improve the positioning solution. Such estimate is typically implemented, again, within the LS framework in order to obtain the so-called *fixed solution*.

The three steps approach for RTK described earlier is known to provide acceptable estimation performance under nominal conditions, which is not the case in urban environments, typically affected by multipath and non-line-of-sight (NLOS) propagation conditions. These harsh propagation conditions are the main source of errors for precise navigation, since the locality of the effect prevents augmentation systems from assisting meaningfully against such channel effects. As a consequence, counter measuring signal reflections can be better done locally at the receiver in either the baseband processing (i.e., in the calculation of observables) or the navigation side (i.e., when producing the PVT solution). In this work, we focus on the later, where the usual RTK pipeline described earlier is enhanced in order to provide additional robustness to local effects. The result is a new RTK technique that is resilient to, for instance, multipath conditions. The key point is to improve the performance of the float solution estimation, where the multipath-contaminated satellite links are detected, enabling the guidance of the integer ambiguity search and enhancing its success ratio. To achieve such goal, we propose to use a robust KF with outlier detection and

rejection capabilities, which is based on concepts from Variational Bayes (VB) inference methods. VB inference is an efficient approximating method to estimate posterior probabilities. The main idea of this method is to come up with a tractable distribution to approximate posterior distribution of latent variables by minimizing Kullback-Leibler divergence. The reason why VB inference is needed is that latent variables is designed to detect and reject outliers, which is also the difference of standard KF and this robust KF. The basic difference between standard KF and VB inference-based KF is the model assumed. In standard KF, only Additive White Gaussian Noise (AWGN) is considered and therefore Gaussian distribution is assumed, in which standard KF is optimal. However, in VB inference-based KF, multipath is also considered in addition to AWGN. With new model built, latent variables is assumed to mitigate multipath's influence, which is why VB inference is applied.

The new approach is validated using real data on a challenging propagation environment. The real data used in this work was recorded during a measurement campaign on 16th May 2017 (DOY 208, UTC 12:00-13:30) conducted in Koblenz (Germany) on the Moselle river. The data was collected on board of a vessel, which travelled through the river with several bridges and a waterway lock, then affected by severe multipath and NLOS conditions. The evaluation comprises the positioning accuracy of the proposed algorithm, alongside with the fixing rate. The fixing rate defines the probability of finding the correct set of integer ambiguities, based on an empirical method aiming to deice whether the estimated set of integer ambiguities can be considered sufficiently more likely than any other integer candidates [8]. The reported results show the added robustness when adding a robust KF in the RTK pipeline.

RTK MODEL

RTK is a relative positioning procedure, where the unknown position of a moving rover station is determined with respect to a stationary base station of known coordinates. Fig. 1 (left) illustrates the working principle. Due to the single-differencing the satellite clock error is completely eliminated, while the satellite orbit error and the atmosphere-related delays can be reduced significantly, depending on the distance between the base and rover positions (p_B and p respectively). Then, a pivot satellite (hereinafter referred using the superscript "r") is chosen for double-differencing, cancelling the delays from the receivers clock offsets. Let us consider n + 1 GNSS satellites observed on a vehicle equipped with a GNSS receiver. The observations for code and phase pseudoranges from the satellite i are given by:

$$\rho^{i} = \|\boldsymbol{p}^{i} - \boldsymbol{p}\| + I^{i} + T^{i} + c\left(dt - dt^{i}\right) + \varepsilon^{i} \tag{1}$$

$$\Phi^{i} = \underbrace{\|\mathbf{p}^{i} - \mathbf{p}\|}_{-\mathbf{u}^{i} \mathbf{p}} - I^{i} + T^{i} + c\left(dt - dt^{i}\right) + \lambda N^{i} + \epsilon^{i}$$

$$\tag{2}$$

where

 ρ^i, Φ^i are the code and phase observations [m],

 p^{i}, p are the positions of the ith satellite and the GNSS receiver respectively,

 u^i is the line-of-sight unit vector from the vehicle to the satellite position,

 I^i is the ionospheric error [m],

 T^i is the tropospheric error [m],

c is the speed of light [299 792 458 m/s]

 dt^i, dt are the satellite and receiver clock offsets [s],

 λ is the carrier phase wavelength [m],

 N^i is unknown number of cycles between the receiver and the satellite,

 ε^i , ϵ^i are the remaining unmodelled errors for the code and phase observations respectively.

As shown in Equation 2, the Euclidean norm between the satellite and receiver positions is often expressed in a linearised form as the product of the line of sight vector $u^{i^{\top}}$ and the position of the receiver. Thus, the mathematical

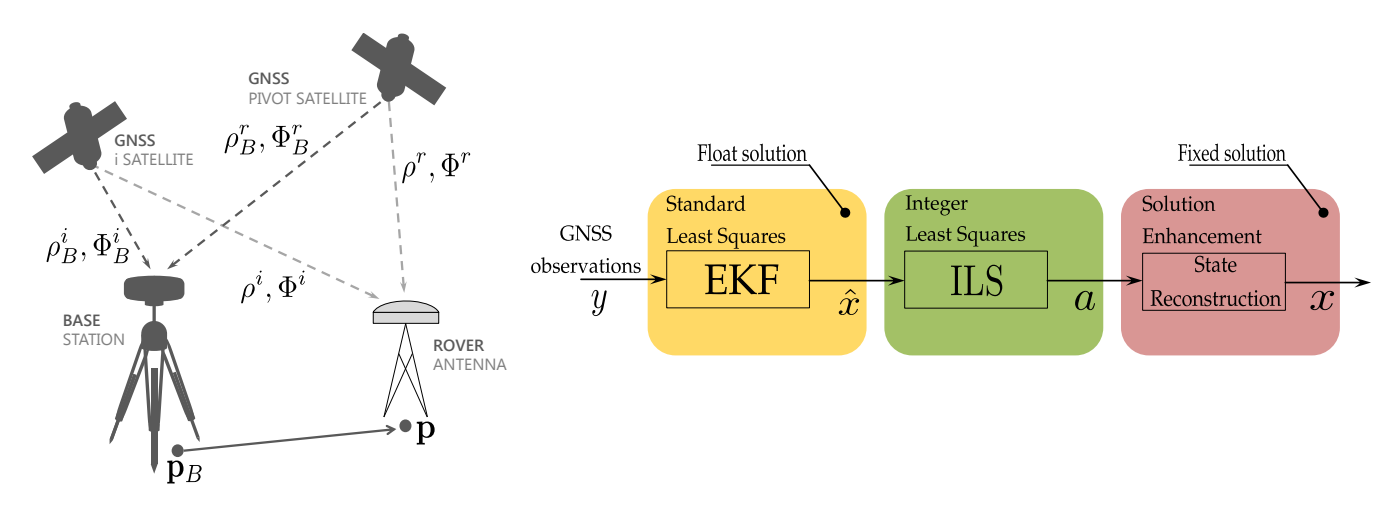


Figure 1: On the right, scheme for the RTK procedure. On the right, the workflow for the ambiguity resolution process.

model of the double-difference code and carrier phase measurements $DD\rho^i$ and $DD\Phi^i$ is

$$DD\rho^{i} = \rho_{j}^{i} - \rho_{m}^{i} - (\rho_{j}^{r} - \rho_{m}^{r})$$

$$= -(\boldsymbol{u}^{i} - \boldsymbol{u}^{r})^{\top} (\boldsymbol{p} - \boldsymbol{p}_{B}) + \varepsilon_{j,b}^{i,r}$$
(3)

$$DD\Phi^{i} = \Phi_{j}^{i} - \Phi_{m}^{i} - (\Phi_{j}^{r} - \Phi_{m}^{r})$$

$$= -(\boldsymbol{u}^{i} - \boldsymbol{u}^{r})^{\top} (\boldsymbol{p} - \boldsymbol{p}_{B}) + \lambda a_{j}^{i} + \epsilon_{j,b}^{i,r}$$
(4)

where the subscript r represents reference satellite, i the observed satellite, j the rover, m the base station and a_j^i is the vector of double-difference ambiguities.

Relating the GNSS observations to a state estimate involves applying a least-squares as

$$\{a, x\} = \min_{\substack{a \in \mathbb{Z}^{n \cdot m} \\ x}} \|y - Aa - Hx\|_{\mathbf{R}}^{2}$$
(5)

where y is the vector of GNSS code and phase observations stacked from every baseline, R is the variance-covariance matrix of the GNSS observations. Given the integer nature of a, the minimization problem of Eq. 5 is generally referred to as Integer Least-Squares (ILS) estimation. Provided that no analytical solution exists to such minimization problem, [7] proposed its decomposition into three-steps procedure of least-squares adjustments.

$$\|\mathbf{y} - A\mathbf{a} - H\mathbf{x}\|_{\mathbf{R}}^2 = \|\hat{\mathbf{e}}\|_{\mathbf{R}}^2 + \|\hat{\mathbf{a}} - \mathbf{a}\|_{P_{\hat{\mathbf{a}}\hat{\mathbf{a}}}}^2 + \|\hat{\mathbf{x}}|a - \mathbf{x}\|_{P_{\hat{\mathbf{x}}|a}}^2$$
 (6)

This procedure is depicted in Fig. 1 (right). The first stage is the computation of a least-squares where the integer constraint of the ambiguities is dropped. The output of this estimation is often referred to as float solution. Then, the estimated float ambiguities and the corresponding variance-covariance matrix is used for the ambiguity resolution process. Then, a ratio test is needed to access the closeness of float ambiguities to the nearest integer vector. The float solutions with ambiguities not close to integer vector enough would be rejected and only those close to integer would be accepted to keep the accuracy of output of ILS, which is also called fixed solution. Finally, the accepted integer ambiguities are used to improve the solution for the vector of dynamical parameters x. Such estimate is realized, once again in a least-squares sense, to obtain the fixed solution. In this work, we focus on the float estimation, where the usual LS or KF is enhanced in order to provide additional robustness to local effects. The result is a new RTK technique that is resilient to, for instance, multipath conditions. The key point is to improve the performance of the float solution estimation, where the multipath-contaminated satellite links are detected, enabling the guidance of the integer ambiguity search and enhancing its success ratio.

ROBUST KALMAN FILTER WITH OUTLIER DETECTION CAPABILITIES

In this section, we first describe the Variation Bayes Kalman filter (VBKF) method for outlier detection and mitigation. The original method estimates the probability of having outliers in the observation at every time step, then down weights that particular observation. Notice that, in the original algorithm, a single indicator z_t is used for all observations gathered at the same time, y_t . In practice, the outliers might affect differently the elements in y_t which is the contribution of this paper, reported in the second subsection below.

Variation Bayes Kalman filter

Standard KF is optimal only in line of sight (LOS) propagation conditions under white noise, however, its performance would degrade in non line of sight (NLOS) scenarios where multipath is considered. To solve this problem and make the KF robust for NLOS conditions, a KF based on VB inference was proposed in [9]. This method can be used in substitution of the KF in the first block of Fig. 1, providing more robust inputs to the Integer LS algorithm.

To introduce the mathematical formulation of the robust KF, a discrete-time state-space model is considered. We assume two possible propagation conditions: i) in the LOS case, observations are affected by AWGN only, ii) in the NLOS case, observations are affected by both AWGN and multipath:

$$x_t = f(x_{t-1}) + \epsilon_t \tag{7}$$

$$y_t = \begin{cases} h(x_t) + \eta_t + M_t & \text{NLOS} \\ h(x_t) + \eta_t & \text{LOS} \end{cases}$$
(8)

where x represents state, y is the observation, $\epsilon \sim \mathcal{N}(\mathbf{0}, \mathbf{Q}_t)$ is the process noise, $\eta \sim \mathcal{N}(\mathbf{0}, \mathbf{R}_t)$ is the measurement noise and M_t is the multipath to mitigate. To make sure that the prediction phase of the KF is not influenced by multipath outliers, the following model is assumed,

$$p(\mathbf{y}_t|\mathbf{x}_t, z_t) = \mathcal{N}(\mathbf{h}(\mathbf{x}_t), \mathbf{R}_t)^{z_t}$$
(9)

where z_t is an outlier indicator which assists in detecting and mitigating the outliers. Particularly, when $z_t = 1$, the model assumes that there are no outliers and the pseudo-range is Gaussian distributed because of the AWGN; when $z_t = 0$, outliers are considered but have limited influence to the estimation phase. Furthermore, we impose a beta-Bernoulli hierarchical prior to the indicator [6],

$$p(z_t|\pi_t) = \pi_t^{z_t} (1 - \pi_t)^{1 - z_t}$$
(10)

where π_t is a beta distribution parameterized by e_0 and f_0 :

$$p(\pi_t) = \frac{\pi_t^{e_0 - 1} (1 - \pi_t)^{f_0 - 1}}{\mathbf{B}(e_0, f_0)}$$
(11)

where $B(\cdot, \cdot)$ is the beta function.

According to Variational Inference [2], $\theta = \{x_t, \pi_t, z_t\}$ is assumed as our latent variables, and we can estimate the posterior distribution $p(\theta|y_{1:t})$ using $q(\theta)$,

$$q(\boldsymbol{\theta}) = q(\boldsymbol{x}_t)q(\pi_t)q(z_t) \tag{12}$$

According to the mean-field Variational Inference method, we can obtain $q(\mathbf{x}_t)$, $q(\pi_t)$ and $q(z_t)$ by calculating the following expectations, respectively,

$$\ln[q(\boldsymbol{x}_t)] = \mathbb{E}_{\pi_t, z_t} \{ \ln[p(\boldsymbol{x}_t, \pi_t, z_t, \boldsymbol{y}_{1:t})] \}$$
(13)

$$\ln[q(\pi_t)] = \mathbb{E}_{\boldsymbol{x}_t, z_t} \{ \ln[p(\boldsymbol{x}_t, \pi_t, z_t, \boldsymbol{y}_{1:t})] \}$$
(14)

$$\ln[q(z_t)] = \mathbb{E}_{\pi_t, \boldsymbol{x}_t} \{ \ln[p(\boldsymbol{x}_t, \pi_t, z_t, \boldsymbol{y}_{1:t})] \}$$
(15)

where

$$p(\boldsymbol{x}_t, \boldsymbol{\pi}_t, z_t, \boldsymbol{y}_{1:t}) \propto p(\boldsymbol{x}_t | \boldsymbol{y}_{1:t-1}) p(\boldsymbol{y}_t | \boldsymbol{x}_t, z_t) p(z_t | \boldsymbol{\pi}_t) p(\boldsymbol{\pi}_t)$$
(16)

In the KF framework, the first term $p(\boldsymbol{x}_t|\boldsymbol{y}_{1:t-1})$ on the right-hand side of (16) is a predictive density, which can be approximated as $p(\boldsymbol{x}_t|\boldsymbol{y}_{1:t-1}) \sim \mathcal{N}(\hat{\boldsymbol{x}}_{t|t-1}, \boldsymbol{P}_{t|t-1})$, where the corresponding mean and covariance are

$$\hat{x}_{t|t-1} = \int f(x_{t-1}) p(x_{t-1}|y_{1:t-1}) dx_{t-1}$$
(17)

$$P_{t|t-1} = \int (f(x_{t-1}) - \hat{x}_{t|t-1})(f(x_{t-1}) - \hat{x}_{t|t-1})^T p(x_{t-1}|y_{1:t-1}) dx_{t-1} + Q_t$$
(18)

with $\hat{x}_{t-1|t-1}$ and $P_{t-1|t-1}$ be the mean and covariance of $p(x_{t-1}|y_{1:t-1}) \sim \mathcal{N}(\hat{x}_{t-1|t-1}, P_{t-1|t-1})$.

Update q(x)

With (13), we can finally get $q(x_t)$ as:

$$q(\mathbf{x}_t) \propto \exp(-\frac{1}{2}||\mathbf{x}_t - \hat{\mathbf{x}}_{t|t-1}||_{\mathbf{P}_{t|t-1}^{-1}}^2 - \frac{\langle z_t \rangle}{2}||\mathbf{y}_t - \mathbf{h}(\mathbf{x}_t)||_{\mathbf{R}_t^{-1}}^2)$$
(19)

where $\langle z_t \rangle$ is the expectation of z_t . Thus, we can see that $q(x_t) \sim \mathcal{N}(\hat{x}_{t|t}, P_{t|t})$, with

$$\hat{\boldsymbol{x}}_{t|t} = \hat{\boldsymbol{x}}_{t|t-1} + \boldsymbol{K}_t(\boldsymbol{y}_t - \hat{\boldsymbol{y}}_{t|t-1})$$
(20)

$$P_{t|t} = P_{t|t-1} - K_t(S_t + \overline{R}_t)K_t^T$$
(21)

$$K_t = C_t (S_t + \overline{R}_t)^{-1} \tag{22}$$

and

$$\hat{\mathbf{y}}_{t|t-1} = \int \mathbf{h}(\mathbf{x}_t) p(\mathbf{x}_t | \mathbf{y}_{1:t-1}) d\mathbf{x}_t$$
(23)

$$S_t = \int (\boldsymbol{h}(\boldsymbol{x}_t) - \hat{\boldsymbol{y}}_{t|t-1})(\boldsymbol{h}(\boldsymbol{x}_t) - \hat{\boldsymbol{y}}_{t|t-1})^T p(\boldsymbol{x}_t|\boldsymbol{y}_{1:t-1}) d\boldsymbol{x}_t$$
(24)

$$C_t = \int (\boldsymbol{x}_t - \hat{\boldsymbol{x}}_{t|t-1})(\boldsymbol{h}(\boldsymbol{x}_t) - \boldsymbol{y}_{t|t-1})^T p(\boldsymbol{x}_t|\boldsymbol{y}_{1:t-1}) d\boldsymbol{x}_t$$
(25)

where $\overline{R}_t = \frac{R_t}{\langle z_t \rangle}$. When outliers occur, $\langle z_t \rangle$ is not close to 1, for example, $\langle z_t \rangle < 1 - 1 \times 10^{-3}$, then we ignore the measurement and simply update:

$$\hat{\boldsymbol{x}}_{t|t} = \hat{\boldsymbol{x}}_{t|t-1} \tag{26}$$

$$P_{t|t} = P_{t|t-1} \tag{27}$$

Update $q(z_t)$

With (15), we have that $q(z_t)$ is

$$q(z_t) \propto \exp\{-0.5z_t \operatorname{Trace}(\boldsymbol{B}_t \boldsymbol{R}_t^{-1}) + z_t \langle \ln[\pi_t] \rangle + (1 - z_t) \langle \ln[1 - \pi_t] \rangle\}$$
(28)

where $\langle \cdot \rangle$ represented the expectation and B_t is given by

$$\boldsymbol{B}_{t} = \int (\boldsymbol{y}_{t} - \boldsymbol{h}(\boldsymbol{x}_{t}))(\boldsymbol{y}_{t} - \boldsymbol{h}(\boldsymbol{x}_{t}))^{T} q(\boldsymbol{x}_{t}) d\boldsymbol{x}_{t}$$
(29)

Thus, z_t is a Bernoulli-distributed parameter with

$$p(z_t = 1) = Ae^{-0.5\operatorname{Trace}(\boldsymbol{B}_t \boldsymbol{R}_t^{-1}) + \langle \ln[\pi_t] \rangle}$$
(30)

$$p(z_t = 0) = Ae^{\langle \ln[1 - \pi_t] \rangle} \tag{31}$$

where A is a normalizing constant. Hence the expectation of z_t , $\langle z_t \rangle$, can be updated as

$$\langle z_t \rangle = \frac{p(z_t = 1)}{p(z_t = 1) + p(z_t = 0)}$$
 (32)

Update $q(\pi_t)$

With (14), we can get $q(\pi_t)$ as

$$q(\pi_t) \propto \exp(e_t \ln[\pi_t] + f_t \ln[1 - \pi_t]) \tag{33}$$

where

$$e_t = e_0 + \langle z_t \rangle \tag{34}$$

$$f_t = f_0 + 1 - \langle z_t \rangle \tag{35}$$

Thus, the robust KF based on variational inference is obtained, in which outliers indicator z_t plays an important role to detect and reject outliers compared with the standard KF. In RTK model, the covariance of measurements, which is R_t in (9), measures the performance of Kalman filter together with ILS method. However, when generating outlier indicator in (28), the B_t from (29) only measures the performance of robust Kalman filter. Note that the ILS method can finally improve the accuracy of Kalman filter from meter level to centimeter level in the case of code observation and even higher in the case of phase observation. Therefore, hyper-parameters e_0 and f_0 are needed to set properly to provide more tolerance to the lower accuracy of robust Kalman filter, to avoid the outlier indicator regards every observations as outliers. For the same reason, the threshold value for $\langle z_t \rangle$ is set around 1 to decide whether to ignore measurements and apply the simplified model (26) and (27).

Independent outlier indicators

In the previous model, double-difference code measurements $DD\rho^i$ are related to each other in the terms of channels or satellites as well as the double-difference carrier-phase measurements $DD\phi^i$, according to equation (3) and (4). However, one outlier indicator for all observations also means a waste of information since the whole observations would be rejected even if not all observations are contaminated with outliers. Therefore, to improve the efficiency of each observation, we assume they are independent measurements for simplified model, and introduce one indicator to each observation. This assumption would cause a model mismatch, and the missing cross-covariance would definitely introduce a loss, however, the improved efficiency of used observations can be a compensate. Thus, the new model is updated as follows:

$$p(\mathbf{y}_t|\mathbf{x}_t, z_t) = \prod_{i=1}^{N} \mathcal{N}(\mathbf{y}_t^{(i)}; \mathbf{h}^{(i)}(\mathbf{x}_t), \mathbf{R}_t^{(i)})^{z_t^{(i)}},$$
(36)

where N is the amount of observed double-difference code or carrier-phase measurements; $y_t^{(i)}$ refers to the ith observation in y_t ; $z_t^{(i)}$ is an indicator for each code or carrier-phase observation, with beta-Bernoulli heretical prior:

$$p(z_t^{(i)}|\pi_t^{(i)}) = \pi_t^{(i)} z_t^{(i)} (1 - \pi_t^{(i)})^{1 - z_t^{(i)}}$$
(37)

where $\pi_t^{(i)}$ is still a beta distribution parameterized by $e_0^{(i)}$ and $f_0^{(i)}$:

$$p(\pi_t^{(i)}) = \frac{\pi_t^{(i)} e_0^{(i)} - 1}{\mathbf{B}(e_0^{(i)}, f_0^{(i)})}$$
(38)

Therefore, the q(x) would be updated as:

$$q(\mathbf{x}_t) \propto \exp(-\frac{1}{2}||\mathbf{x}_t - \hat{\mathbf{x}}_{t|t-1}||_{\mathbf{P}_{t|t-1}^{-1}}^2 - \frac{\langle \mathbf{Z}_t \rangle}{2}||\mathbf{y}_t - \mathbf{h}(\mathbf{x}_t)||_{\mathbf{R}_t^{-1}}^2)$$
 (39)

where Z_t is a diagonal matrix with all $z_t^{(i)}$. Thus, we can see that $q(x_t) \sim \mathcal{N}(\hat{x}_{t|t}, P_{t|t})$, with

$$\hat{x}_{t|t} = \hat{x}_{t|t-1} + K_t(y_t - \hat{y}_{t|t-1})$$
(40)

$$P_{t|t} = P_{t|t-1} - K_t(S_t + \overline{R}_t)K_t^T$$
(41)

$$K_t = C_t (S_t + \overline{R}_t)^{-1}$$
(42)

where $\overline{\boldsymbol{R}}_t = \langle \boldsymbol{Z}_t \rangle^{-1} \boldsymbol{R}_t$.

The update of $q(z_t^{(i)})$ is as:

$$q(z_t^{(i)}) \propto \exp\{-0.5z_t^{(i)}(b_t^{(i)}/r_t^{(i)}) + z_t^{(i)}\langle \ln[\pi_t^{(i)}]\rangle + (1 - z_t^{(i)})\langle \ln[1 - \pi_t^{(i)}]\rangle\}$$

$$\tag{43}$$

where $\langle \cdot \rangle$ represented the expectation, $r_t^{(i)}$ is the *i*th element of the diagonal vector of \mathbf{R}_t and $b_t^{(i)}$ is given by

$$b_t^{(i)} = \int (\boldsymbol{y}_t^{(i)} - \boldsymbol{h}^{(i)}(\boldsymbol{x}_t))(\boldsymbol{y}_t^{(i)} - \boldsymbol{h}^{(i)}(\boldsymbol{x}_t))^T q(\boldsymbol{x}_t) d\boldsymbol{x}_t$$
(44)

Thus, $z_t^{(i)}$ is a Bernoulli-distributed parameter with

$$p(z_t^{(i)} = 1) = Ae^{-0.5(b_t^{(i)}/r_t^i) + \langle \ln[\pi_t^{(i)}] \rangle}$$
(45)

$$p(z_t^{(i)} = 0) = Ae^{\langle \ln[1 - \pi_t^{(i)}] \rangle}$$
 (46)

where A is a normalizing constant. Hence the expectation of $z_t^{(i)}$, $\langle z_t^{(i)} \rangle$, can be updated as

$$\langle z_t^{(i)} \rangle = \frac{p(z_t^{(i)} = 1)}{p(z_t^{(i)} = 1) + p(z_t^{(i)} = 0)} \tag{47}$$

Following the same way above, $q(\pi_t^{(i)})$ is updated as:

$$q(\pi_t^{(i)}) \propto \exp(e_t^{(i)} \ln[\pi_t^{(i)}] + f_t^{(i)} \ln[1 - \pi_t^{(i)}])$$
(48)

where

$$e_t^{(i)} = e_0 + \langle z_t^{(i)} \rangle \tag{49}$$

$$f_t^{(i)} = f_0 + 1 - \langle z_t^{(i)} \rangle \tag{50}$$

VALIDATION AND EXPERIMENTATION

To evaluate the performance of the proposed robust RTK navigation algorithm, a static dataset from Cadiz (Spain) collected by IGS was used. The sampling frequency is 30 Hz and the length of data used is about 33 seconds. To simulate the signal degraded scenarios, bias caused by multipath is simulated based on Markov Chain model and injected into the code observations of certain satellites to bring signal degraded scenarios to double difference code observations. Similarly, cycle slip caused by multipath is simulated based on Markov Chain model and injected into certain phase observations to contaminate double difference phase observations. The bias caused by multipath to one double difference observation is shown as an example in Fig. 2, and the example of bias caused by multipath to one double difference phase observation is shown in Fig. 3.

SIMULATION RESULTS

As a comparison, the robust RTK method as well as the standard RTK method are both applied with the data set. With original raw data set, Fig. 4 shows the ratio tests of standard RTK method (above) and robust RTK method (below), where blue line indicates the ratio result for every epoch, which is used to compared with a 3-valued threshold (red dashed line) to decide the acceptance of Position Velocity and Time (PVT) estimation [8], and orange line shows the case of acceptance or rejection. From Fig. 4, we can find that robust RTK method behaves a bit worse than the standard one in terms of acceptance rate when there is no multipath problem. Besides, according to Fig. 5, the two RTK methods share a similar performance since the two lines in figure match with each other.

As for the simulation of signal degraded scenarios, the results when two double difference code and phase observation are contaminated are shown in Fig. 6 and Fig. 7. According to Fig. 6, we can find that more PVT estimations are provided with robust RTK method under signal degraded scenarios compared with the standard RTK algorithm but the RTK methods still share a similar performance in Fig. 7. Detailed comparison of these two methods are shown in Table. 1 as an average result over 100 Monte Carlo simulations. In terms of missed detection, which is the wrong

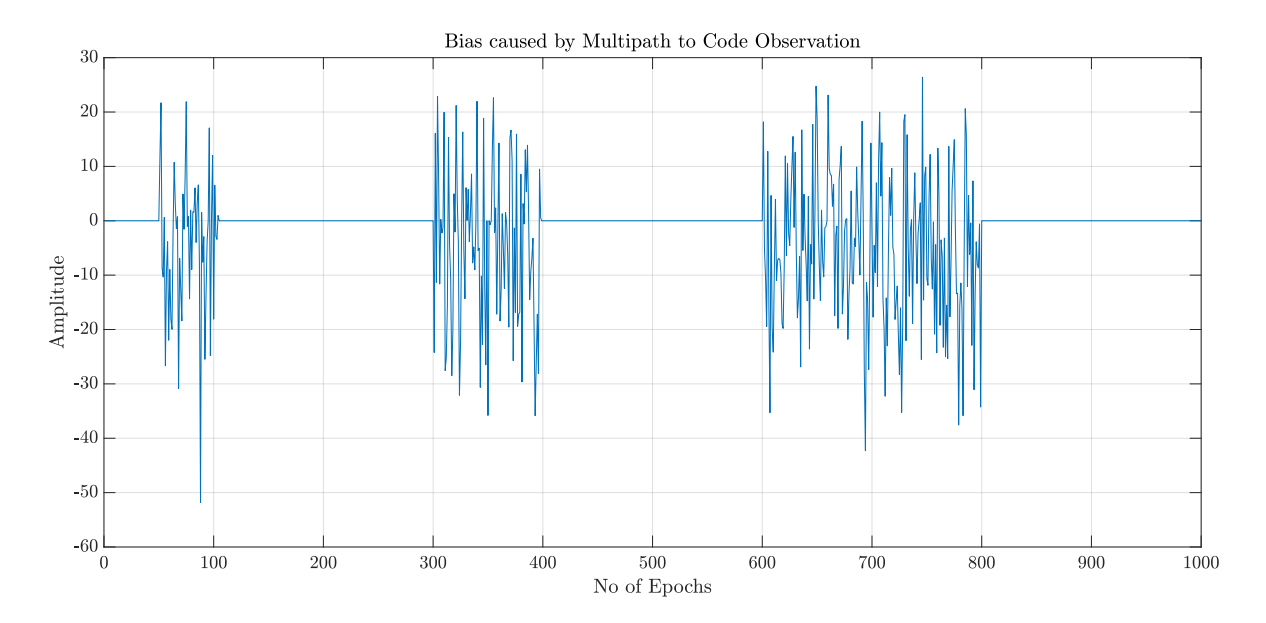


Figure 2: Bias caused by multipath to double difference code observations.

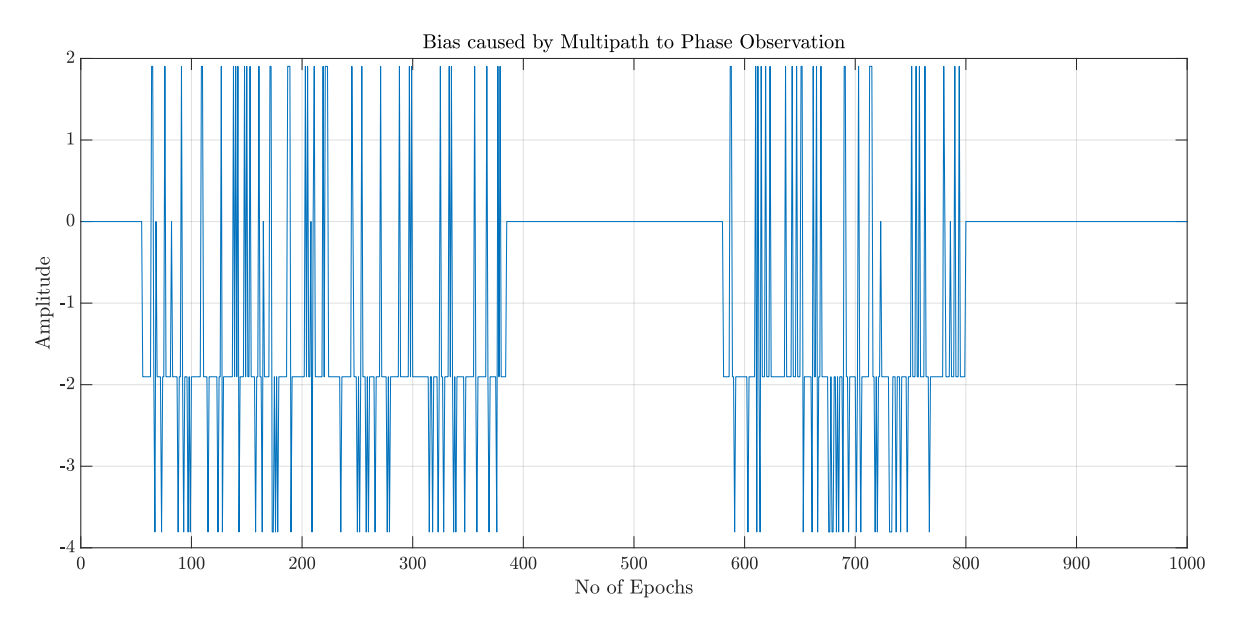


Figure 3: Bias caused by multipath to double difference phase observations.

PVT estimation passing ratio test, the two RTK methods show a similar estimation accuracy. However, in terms of acceptance rate, the robust RTK method holds an obvious advantage against the standard RTK method. With the increase of contaminated observations, the performance of robust RTK method couldn't be held in the same level. Fig. 8 and Fig. 9 show the case when 4 satellites are affected by multipath. According to the two figures, robust RTK method begins to show a degraded performance in terms of acceptance rate, while the two RTK methods still hold a similar performance in terms of estimation accuracy. However, in the table in Fig. 2, we can see a slightly degraded performance with robust RTK method in terms of missed detection, which is caused by the model mismatch because of the independent double difference observation assumption, while the robust RTK method almost holds no advantage against standard RTK method.

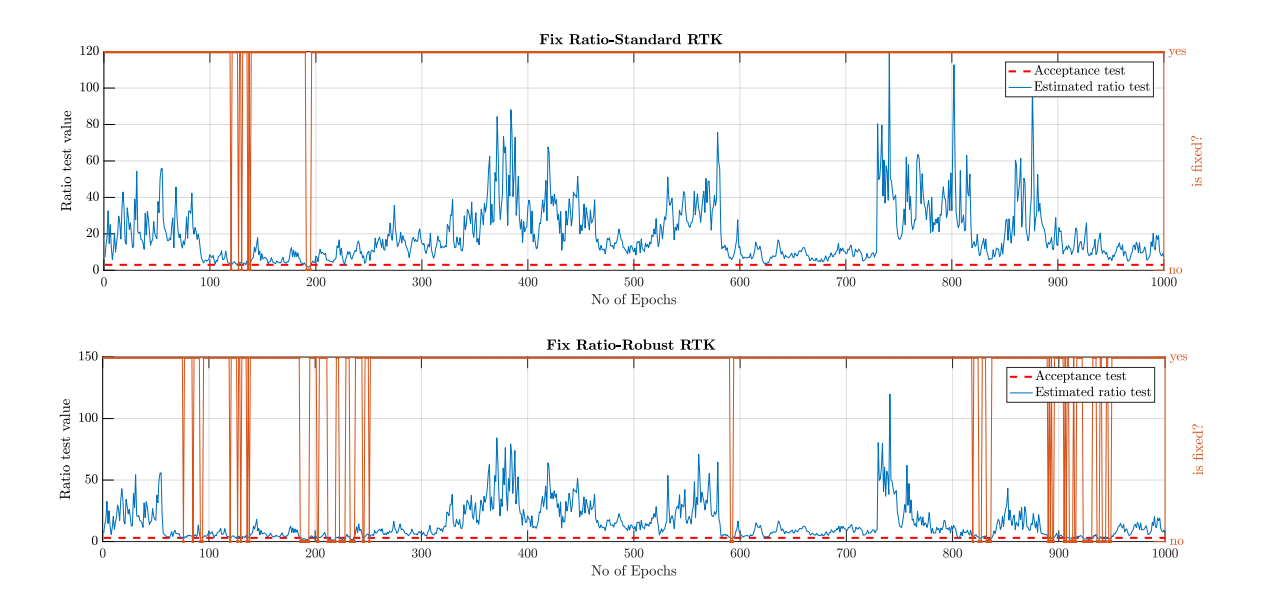


Figure 4: Fix ratio shows how close the ambiguity estimation is to integer, but not exactly to the true value. The orange line is the acceptance test result, with above as acceptance and below as rejection. The blue line indicates the ratio result for every epoch, which is used to compared with a threshold (red dashed line) to decide the acceptance.

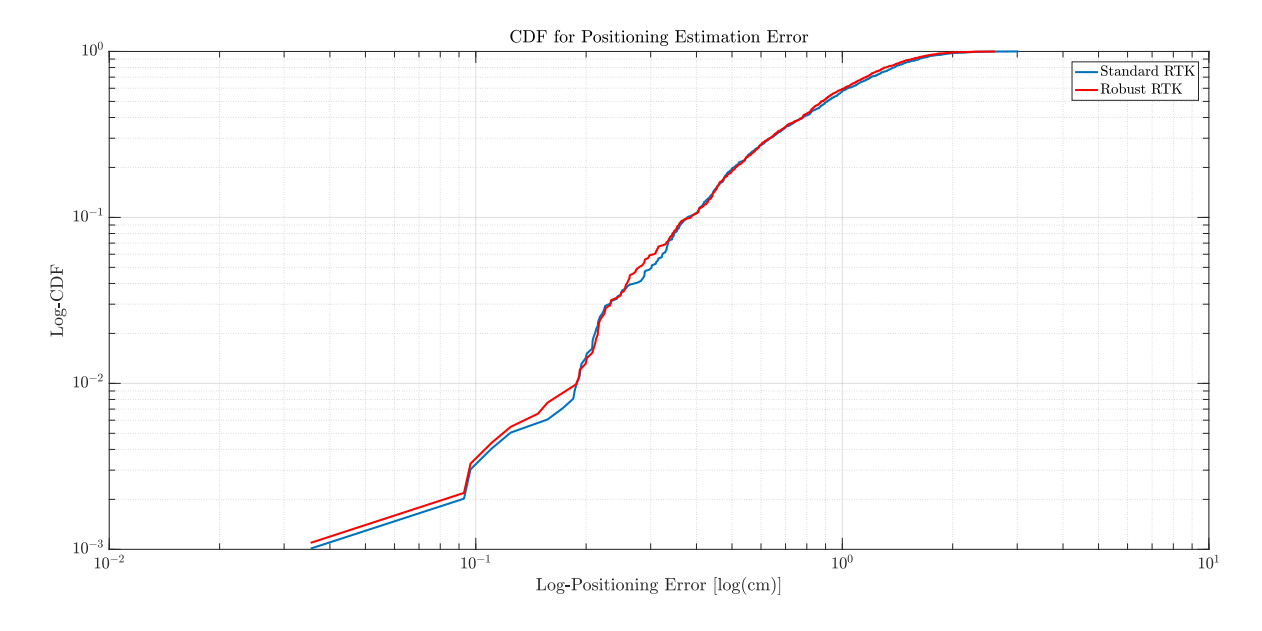


Figure 5: Log of CDF for the fixed position estimation error according to the true one, where the blue line shows the performance of standard RTK method while the red line represents the robust RTK method.

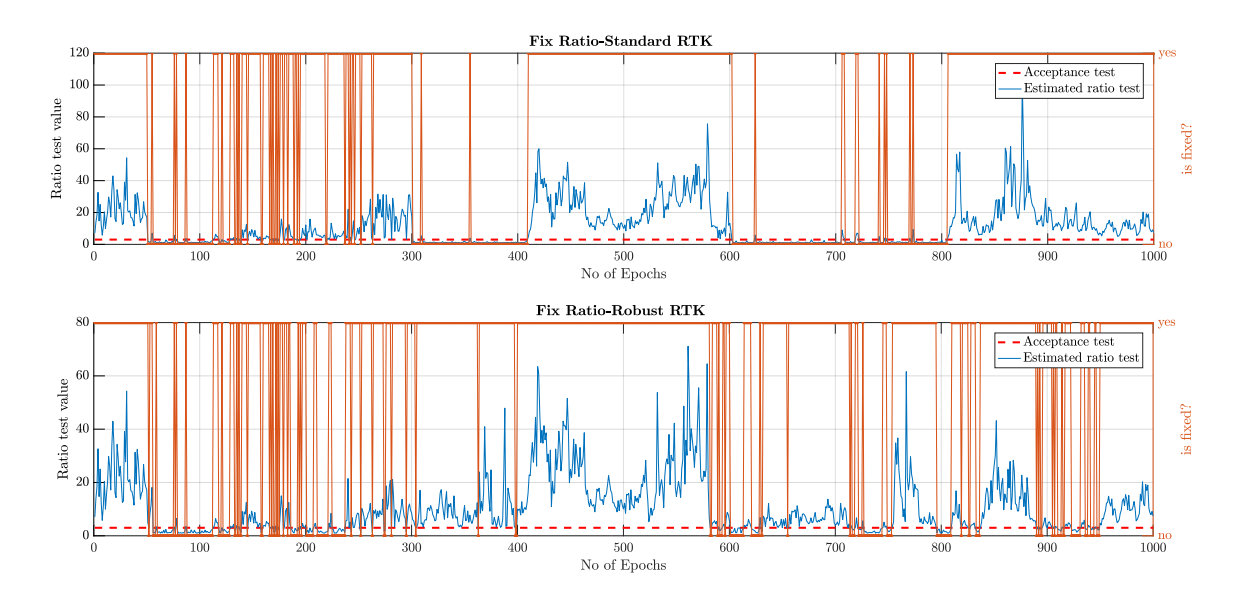


Figure 6: Fix ratio shows how close the ambiguity estimation is to integer, but not exactly to the true value. The orange line is the acceptance test result, with above as acceptance and below as rejection. The blue line indicates the ratio result for every epoch, which is used to compared with a threshold (red dashed line) to decide the acceptance.

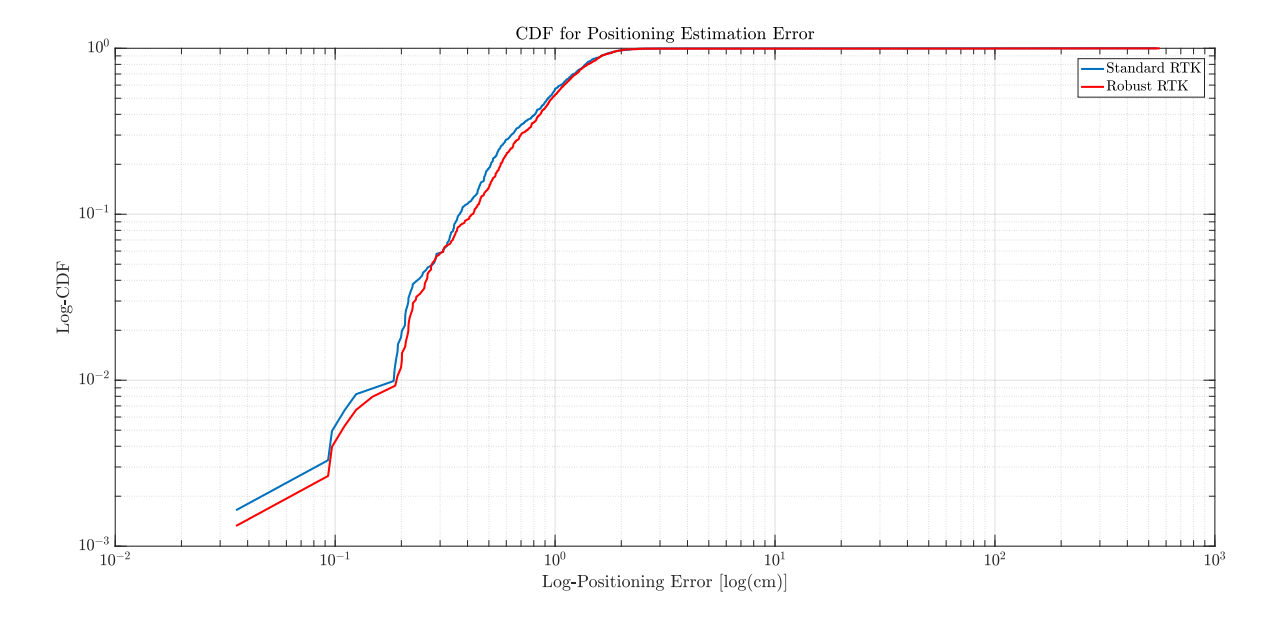


Figure 7: Log of CDF for the fixed position estimation error according to the true one, where the blue line shows the performance of standard RTK method while the red line represents the robust RTK method.

Average over 100	Missed detection rate	Acceptance rate
Monte Carlo Simulation	for contaminated data	for contaminated data
Standard RTK	0.2%	20.94%
Robust RTK	0.27%	64.57%

Table 1: Average result over 100 Monte Carlo simulations when 2 satellites are affected by multipath; missed detection rate represents the PVT estimation that passed the ratio test is still wrong; contaminated data means the data contaminated by multipath; acceptance rate shows the amount of accepted PVT estimations under multipath problem in terms of percentage of contaminated data.

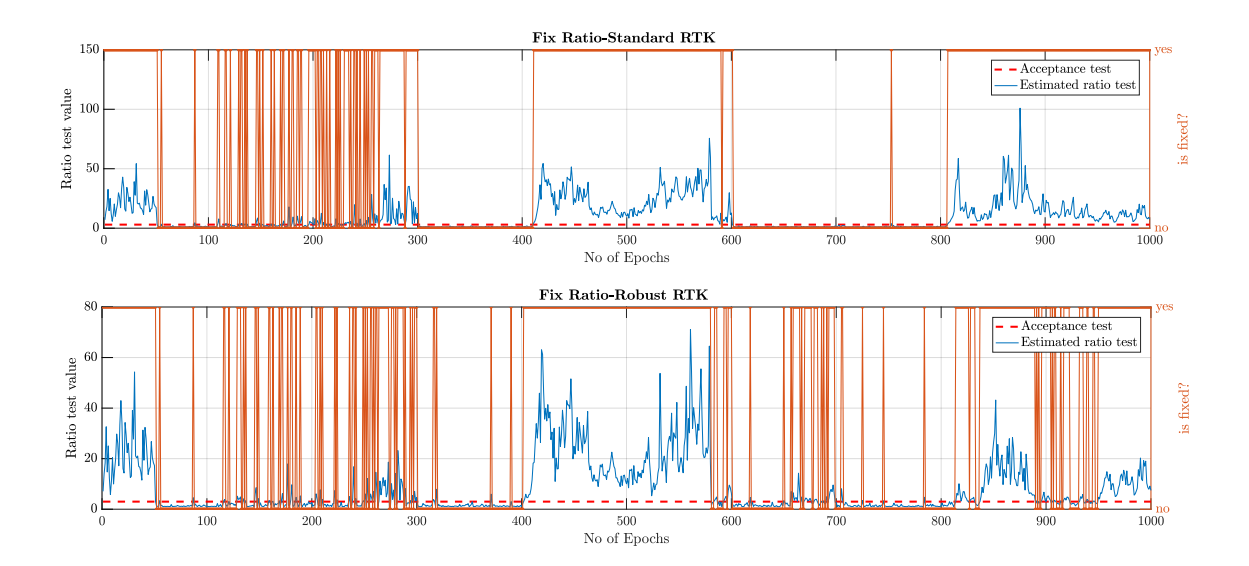


Figure 8: Fix ratio shows how close the ambiguity estimation is to integer, but not exactly to the true value. The orange line is the acceptance test result, with above as acceptance and below as rejection. The blue line indicates the ratio result for every epoch, which is used to compared with a threshold (red dashed line) to decide the acceptance.

Average over 100	Missed detection rate	Acceptance rate
Monte Carlo Simulation	for contaminated data	for contaminated data
Standard RTK	0.3%	20.63%
Robust RTK	0.86%	21.41%

Table 2: Average result over 100 Monte Carlo simulations when 4 satellites are affected by multipath; missed detection rate represents the PVT estimation that passed the ratio test is still wrong; contaminated data means the data contaminated by multipath; acceptance rate shows the amount of accepted PVT estimations under multipath problem in terms of percentage of contaminated data.

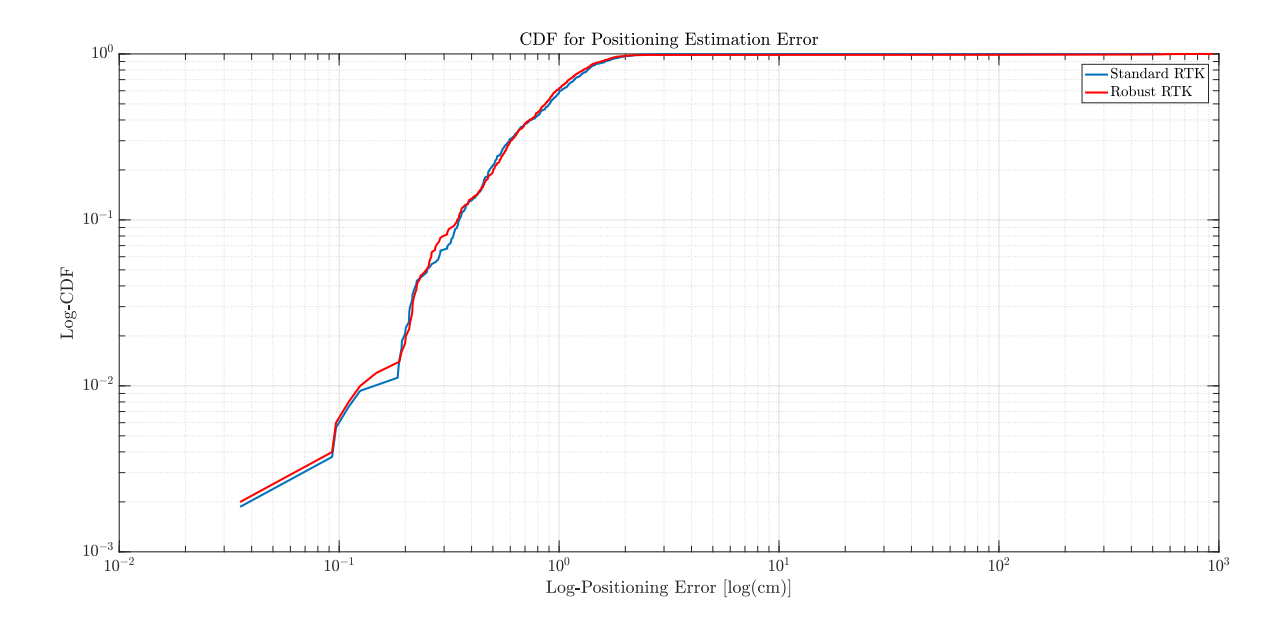


Figure 9: Log of CDF for the fixed position estimation error according to the true one, where the blue line shows the performance of standard RTK method while the red line represents the robust RTK method.

CONCLUSION

This paper presents an innovative approach to improve the acceptance rate of PVT estimations in which robust Kalman filter based on variational inference method is applied to only remove the contaminated double difference observations but leave others for an accurate PVT solution. Performance of robust RTK method are provided by the ratio test result and position estimation error in both experiment (LOS case) and simulations (NLOS case), showing the benefit as well as the limit of RTK algorithm based on robust Kalman filter.

ACKNOWLEDGEMENTS

This work was partially funded by the National Science Foundation under Awards CNS-1815349 and ECCS-1845833, and the 2019 TéSA Research Fellowship.

REFERENCES

- [1] Moeness G Amin, Pau Closas, Ali Broumandan, and John L Volakis. Vulnerabilities, threats, and authentication in satellite-based navigation systems [scanning the issue]. *Proceedings of the IEEE*, 104(6):1169–1173, 2016.
- [2] Christopher M. Bishop. Pattern Recognition and Machine Learning. Springer, 2006.
- [3] Davide Dardari, Pau Closas, and Petar M Djurić. Indoor tracking: Theory, methods, and technologies. *IEEE Transactions on Vehicular Technology*, 64(4):1263–1278, 2015.
- [4] Davide Dardari, Emanuela Falletti, and Marco Luise. Satellite and terrestrial radio positioning techniques: a signal processing perspective. Academic Press, 2011.
- [5] Richard B Langley. RTK GPS. GPS World, 9(9):70-76, 1998.
- [6] Tine Lefebvre, Herman Bruyninckx, and Joris Schutter. Nonlinear Kalman filtering for force-controlled robot tasks, volume 19. Springer, 2005.
- [7] Peter JG Teunissen. Least-squares estimation of the integer GPS ambiguities. In *Invited lecture, section IV theory and methodology, IAG general meeting, Beijing, China*, 1993.
- [8] Sandra Verhagen and Peter JG Teunissen. The ratio test for future GNSS ambiguity resolution. GPS solutions, 17(4):535–548, 2013.
- [9] Hongwei Wang, Hongbin Li, Jun Fang, and Heping Wang. Robust Gaussian Kalman filter with outlier detection. *IEEE Signal Processing Letters*, 25(8):1236–1240, 2018.

[10]	Liang Wang, Zishen Li, Maorong Ge, Frank Neitzel, Zhiyu Wang, and Hong Yuan. Validation and assessment of Multi-GNSS real-time precise point positioning in simulated kinematic mode using IGS real-time service. Remote Sensing, 10(2):337, 2018.